PHYSICAL REVIEW D **93,** 094025 (2016)

η_c elastic and transition form factors: Contact interaction and algebraic model

Marco A. Bedolla, Khépani Raya, J. J. Cobos-Martínez, and Adnan Bashir

Instituto de Física y Matemáticas, Universidad Michoacana de San Nicolás Hidalgo, Edificio C-3, Ciudad Universitaria, Morelia, Michoacán 58040, Mexico

(Received 14 March 2016; published 23 May 2016)

For the flavor-singlet heavy-quark system of charmonia in the pseudoscalar [$\eta_c(1S)$] channel, we calculate the elastic (EFF) and transition form factors (TFFs) [$\eta_c(1S) \to \gamma\gamma^*$] for a wide range of photon momentum transfer squared (Q^2). The framework for this analysis is provided by a symmetry-preserving Schwinger-Dyson equation and Bethe-Salpeter equation treatment of a vector × vector contact interaction. We also employ an algebraic model, developed earlier to describe the light-quark systems. It correctly correlates infrared and ultraviolet dynamics of quantum chromodynamics (QCD). The contact interaction results agree with the lattice data for low Q^2. For $Q^2 \geq Q_0^2$, the results start deviating from the lattice results by more than 20%. $Q_0^2 \approx 2.5$ GeV^2 for the EFF, and $\approx$25 GeV^2 for the TFF. We also present the results for the EFF, TFF, and $\eta_c(1S)$ parton distribution amplitude for the algebraic model. Wherever the comparison is possible, these results are in excellent agreement with the lattice, perturbative QCD, results obtained through a Schwinger-Dyson equation–Bethe-Salpeter equation study, employing refined truncations, and the experimental findings of the *BABAR* experiment.

DOI: 10.1103/PhysRevD.93.094025

I. INTRODUCTION

The internal dynamics of mesons, orchestrated by quantum chromodynamics (QCD), dictates their observable properties. Electromagnetic elastic (EFFs) and transition form factors (TFFs) provide important examples. In experiment, these quantities are extracted through the meson interaction with a virtual photon which probes them at different resolution scales. Several experimental setups such as the *BABAR*, Belle and the upcoming Belle II, and 12 GeV upgrade of the Jefferson Laboratory hold the potential to measure these form factors for a large range of probing photon virtualities. For example, for the $\eta_c(1S) \to \gamma\gamma^*$ transition form factor, *BABAR* has provided us with results in the range of $0 \lessapprox Q^2 \lessapprox 40$ GeV^2.

Within the well-established framework of Schwinger-Dyson (SDEs) and Bethe-Salpeter equations (BSEs), we can investigate the nonperturbative dynamics of the bound states through first principles in the continuum. SDEs for QCD have been extensively applied to deepen our understanding of the light-quark [1–3] and gluon propagators [4–6], quark-gluon and quark-photon interactions [7–14], meson spectra below the masses of 1 GeV, and their static and dynamic properties. The form factors for the light mesons through such studies have been reported in the Refs. [15–22].

The problem of a heavy meson's static properties has been addressed within a consistent rainbow-ladder (RL) truncation of the SDE-BSE kernels with a varying degree of sophistication for the interaction kernels in Refs. [1,23–35] as well as in the lattice-regularized QCD [36]. Furthermore, within the lattice QCD approach, radiative transitions and two photon decays of charmonium have been computed recently with a satisfactorily agreeable comparison with experimental data [36–39].

The extension of the above program to the form factors of heavy mesons in the SDE-BSE approach is not straightforward. It becomes numerically cumbersome as the quark propagator has to be sampled in a large region of the complex plane. However, a few years ago, a simple alternative model was crafted to have a qualitative guideline to study light-meson properties. It was assumed that the quarks interact not via massless vector-boson exchange but instead through a symmetry preserving vector-vector contact interaction (CI) [19–21,40,41]. This interaction is capable of providing a good description of the meson and baryon ground and excited-states masses for light quarks [19,20,40,41]. The results obtained for the static properties through the CI are also quantitatively comparable to those arrived at by employing sophisticated model interactions which mimic QCD closely [27,42–44]. The form factors are expectedly harder, but a qualitative guide is important to make comparison and contrast with real QCD predictions and experiment.

In a previous work [32], we extended this CI model to the heavy-quark sector to obtain the mass spectrum of charmonia and the decay constants for the pseudoscalar and vector channels. In most cases, the agreement achieved with available experimental data was gratifying. The present article applies this model, with exactly the same input parameters, to the computation of form factors associated with the processes $\eta_c\gamma^* \to \eta_c$ and $\eta_c \to \gamma\gamma^*$, namely, η_c EFF and its TFF to $\gamma\gamma^*$, respectively.

In addition to the CI, we also employ a SDE-based algebraic model (AM), introduced in Ref. [45] and refined

later in Ref. [22]. This model was constructed in the light-quarks sector to capture both the infrared and ultraviolet dynamics of QCD in a single, simple, and algebraically maneuverable formalism. It has been successfully employed to gain insight into the internal nonperturbative dynamics of the charged and neutral pions [22,45–47]. We extend it to the case of η_c, calculating the elastic and transition form factors, as well as the η_c parton distribution amplitude (PDA), achieving remarkable agreement with lattice QCD as well as experiment, whenever possible.

This paper is organized as follows. In Sec. II, we present the necessary SDE-BSE tools and ingredients to study mesons and compute the EFFs and the TFFs of charmonia. We summarize the main features of the CI model for the sake of completeness. We also introduce the AM and present its extension for charmonia. Sections III and IV have been dedicated to the computation of η_c EFF and TFF with the CI and AM, providing comparison with lattice QCD, other models, and existing experimental results wherever possible. In Sec. V, we calculate the η_c PDA through the AM and compare it with the lattice QCD and perturbative calculations. Finally, in Sec. VI, we present our conclusions.

II. FORMALISM

Meson bound states appear as poles in a four-point function. The condition for the appearance of such a pole in a particular J^{PC} channel is given by the BSE [48–50]

$$[\Gamma_H(p;P)]_{tu} = \int \frac{\mathrm{d}^4 q}{(2\pi)^4} K_{tu;rs}(p,q;P)\chi(q;P)_{sr}, \quad (1)$$

where $\chi(q;P) = S_f(q_+)\Gamma_H(q;P)S_g(q_-)$; $q_+ = q + \eta P$, $q_- = q - (1-\eta)P$; p (P) is the relative (total) momentum of the quark-antiquark system; S_f is the f-flavor quark propagator; $\Gamma_H(p;P)$ is the meson Bethe-Salpeter amplitude (BSA), where H specifies the quantum numbers and flavor content of the meson; r, s, t, and u represent color, flavor, and spinor indices; and $K(p,q;P)$ is the quark-antiquark scattering kernel. For a comprehensive recent review of the SDE-BSE formalism and its applications to hadron physics, see, for example, Refs. [42,51].

The f-flavor dressed-quark propagator S_f that enters Eq. (1) is obtained as the solution of the quark SDE [52–55]

$$S_f^{-1}(p) = i\gamma\cdot p + m_f + \Sigma_f(p), \quad (2)$$

$$\Sigma_f(p) = \int \frac{\mathrm{d}^4 q}{(2\pi)^4} g^2 D_{\mu\nu}(p-q)\frac{\lambda^a}{2}\gamma_\mu S_f(q)\Gamma^a_\nu(p,q), \quad (3)$$

where g is the strong coupling constant, $D_{\mu\nu}$ is the dressed-gluon propagator, Γ^a_ν is the dressed-quark-gluon vertex, and m_f is the f-flavor current-quark mass. Since the CI, to be defined later, is nonrenormalizable, it is not necessary to introduce any renormalization constant. The chiral limit is obtained by setting $m_f = 0$ [52–54].

Both $D_{\mu\nu}$ and Γ^a_ν satisfy their own SDE, which in turn are coupled to the equations containing higher n-point functions and so on *ad infinitum*. Therefore, the quark SDE, Eq. (2), is only one of the infinite set of coupled nonlinear integral equations. A tractable problem is defined once we have spelled out our truncation scheme, i.e., once the gluon propagator and the quark-gluon vertex are specified.

A. Contact interaction

It has been shown in Refs. [19,20,40,41] that a momentum-independent vector × vector CI is capable of providing a description of light pseudoscalar and vector mesons static properties, quantitatively comparable to those obtained using more refined QCD model interactions [27,42–44]. Furthermore, the π and ρ EFFs [19,21] and TFFs of the π, [20] have also been calculated in this interaction. In a previous work [32], we have employed this interaction to evaluate the mass spectrum of charmonia and the decay constants of the pseudoscalar and vector meson channels. In this article, we apply it to the computation of the EFF and TFF of the η_c. Therefore, we use

$$g^2 D_{\mu\nu}(k) = \frac{4\pi\alpha_{\mathrm{IR}}}{m_g^2}\delta_{\mu\nu} \equiv \frac{1}{m_G^2}\delta_{\mu\nu}, \quad (4)$$

where $m_g = 800$ MeV is a gluon mass scale which is in fact generated dynamically in QCD (see, for example, Ref. [56]) and α_{IR} is a parameter that determines the interaction strength. For the quark-gluon vertex, the rainbow truncation will be used:

$$\Gamma^a_\mu(p,q) = \frac{\lambda^a}{2}\gamma_\mu. \quad (5)$$

Once the elements of the kernel in the quark SDE have been specified, we can proceed to generate and analyze its solution. The general form of the f-flavored dressed-quark propagator, the solution of Eq. (2), can be written in terms of two Lorentz-scalar dressing functions in the following equivalent and convenient forms:

$$S_f^{-1}(p) = \mathrm{i}\gamma\cdot p A_f(p^2) + B_f(p^2) \quad (6)$$

$$= Z_f^{-1}(p^2)(i\gamma\cdot p + M_f(p^2)). \quad (7)$$

In the latter expression, $Z_f(p^2)$ is known as the wave-function renormalization, and $M_f(p^2)$ is the dressed, momentum-dependent quark mass function, which connects current and constituent quark masses [52–54].

Using Eqs. (4) and (5), the quark SDE equation can be written as

$$S_f^{-1}(p) = i\gamma\cdot p + m_f + \frac{4}{3}\frac{1}{m_G^2}\int\frac{d^4q}{(2\pi)^4}\gamma_\mu S_f(q)\gamma_\mu. \quad (8)$$

The solution of Eq. (8) now has the form

$$S_f^{-1}(p) = i\gamma\cdot p + M_f. \quad (9)$$

In other words, for the CI, $Z_f(p^2) = 1$, and M_f is momentum independent. It is because the last term on the right-hand side of Eq. (8) is independent of the external momentum. The mass M_f is determined as the solution of

$$M_f = m_f + \frac{16M_f}{3\pi^2 m_G^2}\int\frac{d^4q}{(2\pi)^4}\frac{1}{q^2+M_f^2}. \quad (10)$$

Since Eq. (10) is divergent, we must adopt a regularization procedure. We employ the proper time regularization scheme [57] and write

$$\frac{1}{q^2+M^2} = \int_0^\infty d\tau e^{-\tau(q^2+M^2)} \to \int_{\tau_{UV}^2}^{\tau_{IR}^2} d\tau e^{-\tau(q^2+M^2)} = \frac{e^{-\tau_{UV}^2(q^2+M^2)} - e^{-\tau_{IR}^2(q^2+M^2)}}{q^2+M^2}, \quad (11)$$

where τ_{IR}^2 and τ_{UV}^2 are, respectively, infrared and ultraviolet regulators. Note that a nonzero value for $\tau_{IR} \equiv 1/\Lambda_{IR}$ implements confinement by ensuring the absence of quark production thresholds [58]. Furthermore, since Eq. (4) does not define a renormalizable theory, $\tau_{UV} \equiv 1/\Lambda_{UV}$ cannot be removed. Instead, it plays a dynamical role and sets the scale for all dimensioned quantities. The importance of an ultraviolet cutoff in Nambu–Jona-Lasinio type models has also been discussed in Refs. [59,60]. Thus,

$$M_f = m_f + \frac{16M_f}{3\pi^2 m_G^2}\mathcal{I}_{01}(M_f^2;\tau_{IR},\tau_{UV}), \quad (12)$$

where

$$\mathcal{I}_{0n}(M^2;\tau_{IR},\tau_{UV}) = \frac{(M^2)^{2-n}}{16\pi^2\Gamma(n)}\Gamma(n-2,\tau_{UV}^2M^2,\tau_{IR}^2M^2), \quad (13)$$

and $\Gamma(a,z_1,z_2)$ is the generalized incomplete gamma function.

B. Axial-vector Ward-Takahashi identity

The phenomenological features of dynamical chiral symmetry breaking (DCSB) in QCD can be understood by means of the axial-vector Ward-Takahashi identity (axWTI). In the chiral limit, it reads

$$-iP_\mu\Gamma_{5\mu}(p;P) = S^{-1}(p_+)\gamma_5 + \gamma_5 S^{-1}(p_-). \quad (14)$$

The axWTI implies a relationship between the kernel in the BSE, Eq. (1), and that in the quark SDE, Eq. (2),

$$\int\frac{d^4q}{(2\pi)^4}K_{tu;rs}(p,q;P)[\gamma_5 S(q_-) + S(q_+)\gamma_5]_{sr} = [\Sigma(p_+)\gamma_5 + \gamma_5\Sigma(p_-)]_{tu}. \quad (15)$$

This relation must be preserved by any viable truncation scheme of the SDE-BSE coupled system, thus constraining the content of the quark-antiquark scattering kernel $K(p,q;P)$ if an essential symmetry of the strong interactions, and its breaking pattern, are to be faithfully reproduced. Satisfying this identity is particularly important when dynamical chiral symmetry breaking dominates the physics.

However, from a practical point of view, Eq. (15) provides a way of obtaining the quark-antiquark scattering kernel, given an expression for the quark self-energy Σ. For the CI under study, Eq. (15) can be easily satisfied. The resulting expression for the quark-antiquark scattering kernel is the RL truncation. This kernel is the leading-order term in a nonperturbative, symmetry-preserving truncation scheme, which is known and understood to be accurate for the pseudoscalar and vector mesons. Moreover, it guarantees electromagnetic current conservation [58],

$$K(p,q;P)_{tu;rs} = -g^2 D_{\mu\nu}(p-q)\left[\frac{\lambda^a}{2}\gamma_\mu\right]_{ts}\left[\frac{\lambda^a}{2}\gamma_\nu\right]_{ru}, \quad (16)$$

where $g^2D_{\mu\nu}$ is given by Eq. (4). Using the interaction that we have specified via Eqs. (4) and (5), the homogeneous BSE for a meson ($\eta = 1$) takes a simple form:

$$\Gamma_H(p;P) = -\frac{4}{3}\frac{1}{m_G^2}\int\frac{d^4q}{(2\pi)^4}\gamma_\mu S_f(q+P)\Gamma_H(q;P)S_g(q)\gamma_\mu. \quad (17)$$

Since the interaction kernel given in Eq. (16) does not depend on the external relative momentum for the CI, a symmetry-preserving regularization will yield solutions which are independent of it. With a dependence on the relative momentum not supported by the CI, the general form of the BSA for the pseudoscalar and vector channels is given in Ref. [61],

$$\Gamma^{\eta_c}(P) = \gamma_5\left[iE^{\eta_c}(P) + \frac{1}{2M}\gamma\cdot PF^{\eta_c}(P)\right], \quad (18)$$

$$\Gamma_\mu^{J/\Psi}(P) = \gamma_\mu^T E^{J/\Psi}(P) + \frac{1}{2M}\sigma_{\mu\nu}P_\nu F^{J/\Psi}(P), \quad (19)$$

where $M = M_c/2$ is a mass scale, with M_c being the solution of Eq. (12). Results for the physical observables are clearly independent of this choice.

Since the BSE is a homogeneous equation, the BSA has to be normalized by a separate condition. In the RL truncation of the BSE, this condition is

$$P_\mu = N_c \frac{\partial}{\partial P_\mu} \int \frac{d^4q}{(2\pi)^4} \mathrm{Tr}[\bar{\Gamma}_H(-Q)S(q_+)\Gamma_H(Q)S(q)], \tag{20}$$

at $Q = P$, with $P^2 = -m_H^2$ (we choose $\eta = 1$). Equation (20) ensures that the residue of the four-point function at the mass pole is unity. Here, Γ_H is the normalized BSA, and $\bar{\Gamma}_H$ is its charge-conjugated version. For every channel, we will rescale Γ_H such that Eq. (20) is satisfied. Furthermore, for the vector channel, there is an additional factor of $1/3$ on the right-hand side to account for all three meson polarizations.

Once the BSA has been normalized canonically with Eq. (20), we can calculate observables from it. For example, the pseudoscalar leptonic decay constant f_{0^-} is defined by

$$P_\mu f_{0^-} = N_c \int \frac{d^4q}{(2\pi)^4} \mathrm{Tr}[\gamma_5\gamma_\mu S(q_+)\Gamma_{0^-}(P)S(q_-)]. \tag{21}$$

Similarly, the vector decay constant f_{1^-} is

$$m_{1^-} f_{1^-} = \frac{N_c}{3} \int \frac{d^4q}{(2\pi)^4} \mathrm{Tr}[\gamma_\mu S(q_+)\Gamma^{1^-}_\mu S(q_-)], \tag{22}$$

where m_{1^-} is the mass of the vector bound state, and the factor of 3 in the denominator comes from summing over the three polarizations of the spin-1 meson.

1. Corollary of the axial-vector WTI

There are further nontrivial consequences of the axWTI and the CI. They define our regularization procedure, which must maintain

$$\begin{aligned} 0 &= \int \frac{d^4q}{(2\pi)^4} \left[\frac{P\cdot q_+}{q_+^2 + M_f^2} - \frac{P\cdot q_-}{q_-^2 + M_g^2} \right] \\ &= \int_0^1 dx \int \frac{d^4q}{(2\pi)^4} \frac{\frac{1}{2}q^2 + \mathfrak{M}^2}{(q^2 + \mathfrak{M}^2)^2}, \end{aligned} \tag{23}$$

where $\mathfrak{M}^2 = M_f^2 x + M_g^2(1-x) + x(1-x)P^2$. This ensures that Eq. (14) is satisfied. Equation (23) states that the axWTI is satisfied if, and only if, the model is regularized so as to ensure there are no quadratic or logarithmic divergences. Unsurprisingly, these are the circumstances under which a shift in integration variables is permitted, an operation required in order to prove Eq. (14) [19,20,40,41]. The constraint given by Eq. (23) will be implemented in all our calculations so that Eq. (14) is unequivocally preserved.

TABLE I. Ground-state charmonia masses obtained with the best-fit parameter set: $m_g = 0.8$ GeV, $\alpha_{\mathrm{IR}} = 0.93\pi/20$, $\Lambda_{\mathrm{IR}} = 0.24$ GeV, and $\Lambda_{\mathrm{UV}} = 2.788$ GeV. The current-quark mass is $m_c = 0.956^*$ GeV, and the dynamically generated constituent-like mass is $M_c = 1.497$ GeV. Dimensioned quantities are in GeV. (* = This parameter set was obtained from the best fit to the mass and decay constant of the pseudoscalar and vector channels). The average percentage error, with respect to experimental data, is 1.14%.

	Masses			
	$m_{\eta_c(1S)}$	$m_{J/\Psi(1S)}$	$m_{\chi_{c_0}(1P)}$	$m_{\chi_{c_1}(1P)}$
Experiment [67]	2.983	3.096	3.414	3.510
Contact interaction	2.950*	3.129	3.407	3.433
JM [1]	2.821	3.1	3.605	⋯
BK [26]	2.928	3.111	3.321	3.437
RB1 [31]	3.065	⋯	⋯	⋯
RB2 [31]	3.210	⋯	⋯	⋯
FKW [33]	2.925	3.113	3.323	3.489

C. Contact interaction for charmonia

In a recent work [32], we have developed a CI model for charmonia. The results for the low-lying mass spectrum of corresponding mesons are presented in Table I. They are in excellent agreement with experimental data (with an average percentage error of 1.14%) and, consequently, with the findings of more sophisticated SDE-BSE model calculations [26,31,33–35] and lattice QCD computations [62,63]. The fact that a RL truncation with a CI describes the mass spectrum of ground-state charmonia so well can be understood in a simple way: since the wave function renormalization and quark mass function are momentum independent, the heavy quark–gluon vertex can reasonably be approximated by a bare vertex. The decay constants calculated in Ref. [32] for the η_c and J/Ψ channels are given in Table II. For the pseudoscalar meson, the result is in decent agreement with the lattice QCD result. Though it is not exactly the case for the vector channel, it is one of the best results in such models (see Ref. [32] for an extended discussion). Note that the results presented in Tables I and II correspond to a minimal extension of the CI model developed primarily for the light quarks in

TABLE II. The decay constants for the states $\eta_c(1S)$ and $J/\Psi(1S)$ obtained with $m_g = 0.8$ GeV, $\alpha_{\mathrm{IR}} = 0.93\pi/20$, $\Lambda_{\mathrm{IR}} = 0.24$ GeV, and $\Lambda_{\mathrm{UV}} = 2.788$ GeV. The current-quark mass is $m_c = 0.956$ GeV. Dimensioned quantities are in GeV.

	Decay constants	
	f_{η_c}	$f_{J/\Psi}$
Lattice QCD	0.395 [68]	0.405 [69]
S1rp [30]	0.239	0.198
S3ccp [30]	0.326	0.330
BK [26]	0.399	0.448
Contact interaction	0.305	0.220

Refs. [19,20,40,41]. A naive application of this earlier model to quarkonia yielded unacceptable results. The reason can be traced back to the fact that the decay constant is influenced by the high momentum tails of the dressed-quark propagator and the BSAs [3,29,64]. These tails probe the wave function of quarkonia at the origin. Contrastingly, the CI yields a constant mass with no perturbative tail for large momenta. Therefore, this artifact of quarkonia had to be built into the model in an alternative manner. Furthermore, we know that, as the masses become higher, mesons become increasingly pointlike in configuration space. The closer the quarks get, the weaker is the coupling strength between them. We thus extended the CI model by reducing the effective coupling $\alpha_{\rm IR}$, accompanied by an appropriate increase in the ultraviolet cutoff. However, we retained the parameters m_g and $\Lambda_{\rm IR}$ of the light sector since modern studies of the gluon propagator indicate that in the infrared the dynamically generated gluon mass scale virtually remains unaffected by the introduction of heavy dynamical quark masses; see, for example, Refs. [65,66]. In the subsequent sections, we shall use this extended CI to evaluate the η_c EFF and TFF to $\gamma^*\gamma$.

D. Algebraic model for charmonia

We also consider the SDE-based algebraic model, with a simple extension to the heavy-quark sector,

$$\begin{aligned} S^{-1}(p) &= \mathrm{i}\gamma\cdot p + M, \\ \rho_\nu(z) &= \frac{\Gamma(\frac{3}{2}+\nu)}{\Gamma(\frac{1}{2})\Gamma(1+\nu)}(1-z^2)^\nu, \\ \Gamma_{\eta_c}(k;P) &= \mathrm{i}\gamma_5\mathcal{N}\frac{M}{f_{\eta_c}}\int_{-1}^{1}\mathrm{d}z\rho_\nu(z)\frac{M^2}{(k+z\sigma P/2)^2+M^2}, \end{aligned} \tag{24}$$

where $P^2=-m_{\eta_c}^2$. $\mathcal{N}$ plays the role of the canonical normalization condition, Eq. (20), and M is fixed such that $f_{\eta_c}=0.361\,\mathrm{GeV}$ and $\sigma=m_\pi/m_{\eta_c}$. A small σ suppresses the angular dependence $k\cdot P$ of the BSA, characteristic of heavy mesons, while $\sigma=1$ recovers the SDE-based AM for the pion [22].

The parameter ν that appears in Eq. (24) strongly influences the form of the resulting PDA [22]. For the pion, $\nu=1$ produces $\phi_\pi\sim x(1-x)$. This expression is in agreement with the asymptotic QCD prediction. $\nu=-1/2$ yields $\phi_\pi\sim\sqrt{x(1-x)}$, in keeping with a realistic PDA at the hadronic scale [45,70,71]. As the PDA of the pion plays a crucial role in determining the asymptotic behavior of its EFF and the TFF to $\gamma^*\gamma$, the AM is an efficient model to encode both its nonperturbative and asymptotic dynamics, as exemplified in Ref. [22]. This model has also been used to calculate a pion's valence dressed-quark generalized parton distribution (GPD) $H_\pi^v(x,\xi,t)$ for "skewness" $\xi=0$, [47].

Owing to the above discussion about the form of the pion PDA and its relation to the ν parameter, we fix $\nu=1$ for the AM to study the η_c, Eq. (24). Once the AM parameters have been fixed, through the values of m_{η_c}, f_{η_c}, and ν, one can use it to calculate the EFF and TFF for η_c.

E. Electromagnetic interaction: Quark-photon vertex

The interaction of a virtual photon with a meson probes its internal structure and dynamics. The impulse approximation allows electromagnetic processes to be described in terms of quark propagators, bound-state BSAs, and the quark-photon vertex. In combination with the RL truncation for the quark propagator and vertices, it ensures electromagnetic current conservation [15,17,72–74]. Phenomenologically, this approximation has proven to be very successful in describing EFFs and TFFs of light pseudoscalar and vector mesons [15–17].

The coupling of a photon with the bound state's charged constituent is given by the quark-photon vertex. In addition to being determined by its own SDE, which is highly nontrivial to solve, the quark-photon vertex $\Gamma_\mu(p_+,p_-;Q)$ is constrained by the gauge invariance of quantum electrodynamics (QED) through the vector Ward-Takahashi identity (WTI)

$$\mathrm{i}Q_\mu\Gamma_\mu(p_+,p_-;Q)=S^{-1}(p_+)-S^{-1}(p_-). \tag{25}$$

Preserving this identity, and its $Q\to 0$ limit, is key to the conservation of electromagnetic current. In our present truncation, the SDE for the quark-photon vertex, consistent with Eq. (16) (truncated at the RL level), is

$$\Gamma_\mu(p;Q)=\gamma_\mu-\frac{4}{3}\frac{1}{m_G^2}\int\frac{\mathrm{d}^4q}{(2\pi)^4}\gamma_\alpha S(q_+)\Gamma_\mu(q;Q)S(q_-)\gamma_\alpha, \tag{26}$$

where $q_+=q+Q$ and $q_-=q$. Noting that the right-hand side is independent of the relative momenta, the general form of the quark-photon vertex is

$$\Gamma_\mu(Q)=\gamma_\mu^T P_T(Q^2)+\gamma_\mu^L P_L(Q^2), \tag{27}$$

where $Q_\mu\gamma_\mu^T=0$, $\gamma_\mu^T+\gamma_\mu^L=\gamma_\mu$. Furthermore, note that with the usage of Eq. (9) and Eq. (27) the vector WTI is trivially obeyed. Moreover, the bare vertex γ_μ also satisfies the WTI for the contact interaction propagator Eq. (9). However, the bare vertex does not contain vector meson poles, which are relevant for the correct description of the charge interaction radius; see, for example, Ref. [73].

Taking appropriate Dirac traces, and using the constraint of Eq. (23), which stems from the axWTI, we find $P_L(Q^2)=1$ and

$$P_T(Q^2)=\frac{1}{1-K_{J/\Psi}(Q^2)}, \tag{28}$$

where $K_{J/\Psi}$ is the Bethe-Salpeter bound-state kernel in the vector channel, Eq. (19), in the present truncation [32]. Thus, because of the dressing of the quark-photon vertex, our form factors (EFF and TFF) will have a pole at $Q^2 = -m_{J/\Psi}^2$, where $m_{J/\Psi}$ is the vector meson mass.

In the computation of the η_c EFF and TFF in the AM, we use the *ansatz* for the quark-photon vertex as given in Eq. (8) of Ref. [22]. It has earlier been employed successfully in the description of the pion EFF and TFF. Such a form is derived through the gauge technique. It satisfies the WTI, is free of kinematic singularities, reduces to the bare vertex in the free-field limit, and has the same Poincaré transformation properties as the bare vertex.

III. η_c ELASTIC FORM FACTOR

Charge-conjugation eigenstates do not have EFFs. At the quark level of a meson, this can be attributed to the equal and opposite charge of the quark and the corresponding antiquark. Nonetheless, by coupling a vector current to the quarks inside, one can measure a "form factor" that gives information about the internal structure of the state.

The η_c meson, analogously to the pion, has only one vector form factor $F_{\eta_c}(Q^2)$, defined by the $\eta_c\gamma^*$ vertex

$$\Lambda_\mu^{\eta_c\gamma^*}(P_i, P_f; Q) = F_{\eta_c}(Q^2)(P_f + P_i)_\mu, \tag{29}$$

where $Q = P_f - P_i$ is the momentum of the virtual photon and $F_{\eta_c}(Q^2)$ is the η_c EFF, the information carrier of the internal electromagnetic structure of the bound state. In our approach, the impulse approximation for the $\eta_c\gamma^*$ vertex reads

$$\Lambda_\mu^{\eta_c\gamma^*}(P, Q) = 2N_c \int \frac{\mathrm{d}^4k}{(2\pi)^4} \mathrm{Tr}[\mathrm{i}\Gamma_{\eta_c}(-P_f)S(k_2)\mathrm{i}\Gamma_\mu(Q) \times S(k_1)\mathrm{i}\Gamma_{\eta_c}(P_i)S(k)], \tag{30}$$

where $P_i = P - Q/2$ and $P_f = P + Q/2$ are the incoming and outgoing meson momenta, respectively; $Q = P_f - P_i$ is the virtual photon momentum; and the distribution of momentum between the constituents is such that $k_1 = k + P - Q/2$ and $k_2 = k + P + Q/2$. Since the scattering is elastic, $P_i^2 = P_f^2 = -m_H^2$. In terms of P and Q, these constraints are cast as $P \cdot Q = 0$ and $P^2 + Q^2/4 = -m_H^2$, where m_H is the mass of the bound state.

In Fig. 1, we present our results for the η_c EFF, displayed with and without the dressing of the quark-photon vertex. Evidently, this dressing has a negligible effect on the EFF. In other words, in the CI, the heavy quark–photon vertex is almost the bare one for the Q^2 range shown. However, although the timelike sector has not been displayed in Fig. 1, the η_c form factor has a pole at $Q^2 = -m_{J/\Psi}^2$, where $m_{J/\Psi}$ is the mass of the vector bound state; see Table I. This is a consequence of dressing the quark-photon vertex

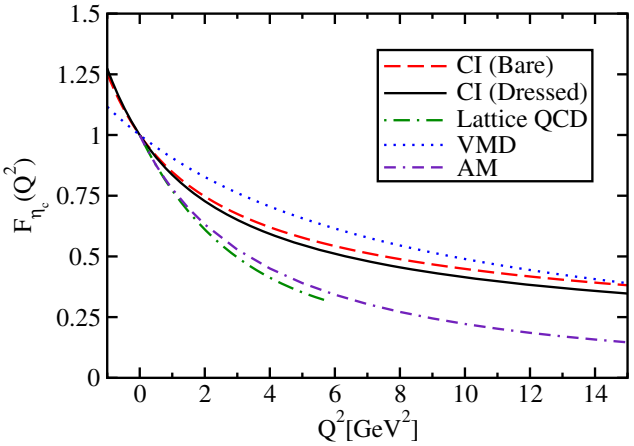

FIG. 1. CI results for the η_c elastic form factor with and without the dressing of the quark-photon vertex. The lattice QCD curve is from Ref. [37], and the VMD monopole result is defined by the mass scale $m_V = 3.096$ GeV. We also include the result obtained with the AM; see Eq. (24).

appropriately. Our results compare well with the vector meson dominance (VMD) model for $Q^2 > 5$ GeV^2 but are harder than the ones predicted by the lattice QCD. Beyond $Q^2 \gtrsim 2.5$ GeV^2, the CI EFF starts deviating from the lattice QCD findings by more than 20%. Notice that the lattice QCD curve is a fit to the data [37], computed in the quenched approximation by assuming the form $F_{\eta_c}(Q^2) = \exp[-\frac{Q^2}{16\beta^2}(1 + \alpha Q^2)]$, where $\beta = 0.480(3)$ GeV and $\alpha = -0.046(1)$ GeV^{-2} on the range $[0, 5.5]$ GeV^2.

We also compute the η_c EFF using the AM, defined through Eqs. (24). Just as for the case of pion EFF, this model fares very well as compared to the lattice results in all the range of virtual photon momentum transfer squared Q^2. The large Q^2 dependence of the EFF is $1/Q^2$ in contrast with the corresponding asymptotic behavior obtained through the CI, which is a constant for $Q^2 \to \infty$. It is already known that the asymptotic form factors obtained through the CI are harder than the QCD predictions [19–21].

In Fig. 2, we compare the η_c EFF with that of the π, both in the RL approximation with a CI and a dressed quark-photon vertex. In both cases, the respective EFF tends to a constant for $Q^2 \to \infty$, which is a consequence of the momentum independence of the interaction. Note that the pion EFF increases more steeply for $Q^2 < 0$ since the pole (the ρ pole for the pion EFF) associated with the dressing of the light quark–photon vertex lies very close to $Q^2 = 0$.

The η_c meson EFF, shown in Fig. 2, can be parameterized by the following functional form in the Q^2 range shown:

$$F_{\eta_c}(Q^2) = \frac{1 + 0.167Q^2 + 0.004Q^4}{1 + 0.372Q^2 + 0.028Q^4}. \tag{31}$$

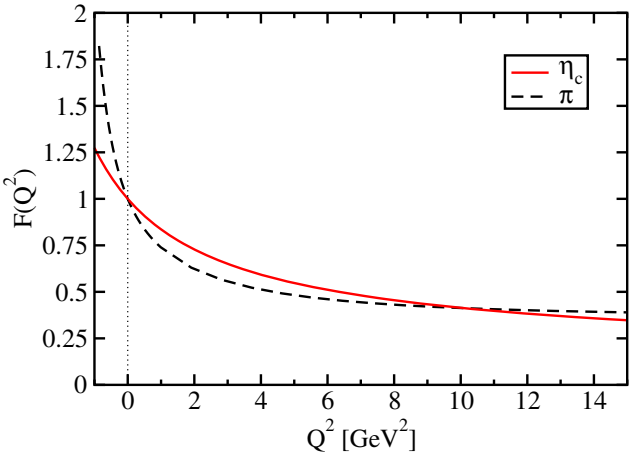

FIG. 2. CI results for the η_c and π elastic form factors. The parameter set used for the calculation of the η_c form factor is that used to produce Tables (I and II) and Fig. 1, while the one used to compute the π form factor is that given in Ref. [21].

Our values for the η_c charge radius, defined by

$$r_{\eta c}^2 = -6\frac{\mathrm{d}F_{\eta_c}(Q^2)}{\mathrm{d}Q^2}\bigg|_{Q^2=0}, \tag{32}$$

are presented in Table III. As can be seen, these compare well with the ones obtained with the more sophisticated Maris-Tandy model interaction [24] and with lattice-regularized QCD [37]. Furthermore, we can compare the charge radius of η_c with that of π, $r_\pi = 0.45$ fm, computed in Ref. [21]. Obviously, $r_{\eta_c} < r_\pi$; i.e., the heavier the meson, the closer it is to being a point particle. We also report the η_c charge radius using the algebraic model AM, Eqs. (24). Expectedly, its prediction lies higher than the CI model (which produces form factors harder than the ones computed in real QCD) and is in line with the result of lattice QCD. Furthermore, the charge radius result, presented in Table III, is also in excellent agreement with the lattice QCD.

IV. $\gamma\gamma^* \to \eta_c$ TRANSITION FORM FACTOR

The interaction vertex describing the $\gamma^*\gamma \to \eta_c$ transition can be parametrized by just one form factor $G_{\gamma^*\gamma\eta_c}(Q_1^2, Q_2^2)$, which can be computed from

TABLE III. The charge radius for the state $\eta_c(1S)$ with the CI and various other calculations. The parameter set used to produce the CI results is that used for Tables (I and II) and Fig. 1. We also include the VMD result with a mass scale $m_V = 3.096$ GeV. The value in parentheses is obtained when we use the bare quark-photon vertex. We have also computed the η_c charge radius using the AM, Eqs. (24).

η_c charge radius (fm)				
SDE [24]	Lattice QCD [37]	VMD	CI	AM
0.219	0.25	0.156	0.219 (0.210)	0.256

$$\mathcal{T}_{\mu\nu}(Q_1, Q_2) = T_{\mu\nu}(Q_1, Q_2) + T_{\nu\mu}(Q_2, Q_1), \tag{33}$$

where Q_1 and Q_2 are the incoming photon momenta, $P = Q_1 + Q_2$ is the η_c momentum, and

$$\begin{aligned} T_{\mu\nu}(Q_1, Q_2) &= \frac{\alpha_{\mathrm{em}}}{\pi f_{\eta_c}} \epsilon_{\mu\nu\alpha\beta} Q_{1\alpha} Q_{2\beta} G_{\gamma^*\gamma\eta_c}(Q_1^2, Q_2^2) \\ &= \mathrm{Tr} \int \frac{\mathrm{d}^4k}{(2\pi)^4} S(k_1)\Gamma_{\eta_c}(k_1, k_2; P) S(k_2) \\ &\quad \times \mathrm{i}\mathcal{Q}_c \Gamma_\mu(k_2, k_3; Q_2) S(k_3) \mathrm{i}\mathcal{Q}_c \Gamma_\nu(k_3, k_1; Q_1), \end{aligned} \tag{34}$$

with $k_1 = k - Q_1$, $k_2 = k + Q_2$, $k_3 = k$, $\mathcal{Q}_c = (2/3)e$, and $\alpha_{\mathrm{em}} = e^2/(4\pi)$. The kinematic constraints are $Q_1^2 = Q^2$, $Q_2^2 = 0$, and $Q_1 \cdot Q_2 = -(m_{\eta_c}^2 + Q^2)/2$, where $P^2 = -m_{\eta_c}^2$, with m_{η_c} the η_c mass.

In Fig. 3, we present the CI results for the $\gamma^*\gamma \to \eta_c$ TFF. Although not shown in Fig. 3, the form factor has a pole at $Q^2 = -m_{J/\Psi}^2$, where $m_{J/\Psi}$ is the mass of the vector bound state. The results compare fairly well with the *BABAR* data and lattice QCD for low Q^2. For this reason, the interaction radius of the transition form factor, defined in Eq. (32) and tabulated in Table IV, compares well with the lattice QCD and *BABAR* findings, as it probes the slope of the TFF for $Q^2 \to 0$. However, for intermediate to large Q^2, CI provides a harder form factor, and the correct asymptotic Q^2 behavior is not captured; see also Fig. 4.

Both the EFF and TFF obtained from the CI and displayed in Figs. (1 and 3) tend to a constant when $Q^2 \to \infty$. This is because the quark propagator mass

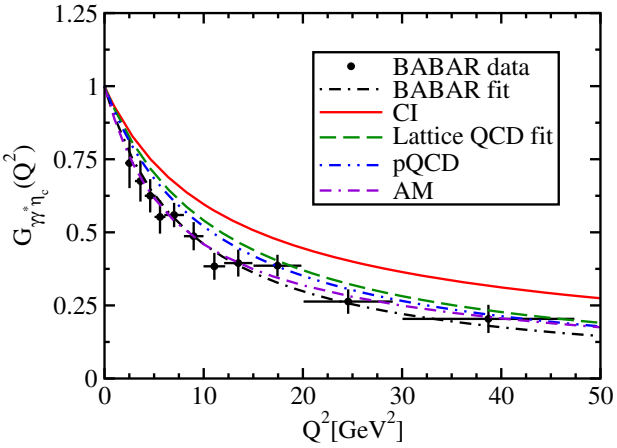

FIG. 3. CI for the transition $\gamma^*\gamma \to \eta_c$ form factor. The lattice QCD curve is a fit [37] to data of the form $G_{\gamma^*\gamma\eta_c}^{\mathrm{Lattice}}(Q^2) = \frac{\mu^2}{\mu^2+Q^2}$ with $\mu = 3.43$ GeV, while the *BABAR* data is a fit [39] of the form $G_{\gamma^*\gamma\eta_c}^{\mathrm{BABAR}}(Q^2) = \frac{1}{1+Q^2/\Lambda}$ with $\Lambda = 8.5$ GeV^2. The perturbative QCD (pQCD) limit is due to Feldmann and Kroll [75]. We also include the plot obtained with the algebraic model; see Eq. (24).

TABLE IV. Interaction radius of the transition $\gamma^*\gamma \to \eta_c$ form factor as defined in Eq. (32). The *BABAR* and lattice QCD results were extracted from their respective monopole parametrization of the data. We also report the results obtained with the AM, Eq. (24).

Interaction radius (fm)			
BABAR [39]	Lattice QCD [37]	CI	AM
0.166	0.141	0.133	0.17

function and BSAs are momentum independent, which is a characteristic of the CI; see Eq. (4). The need thus arises to calculate these objects, and the resulting form factors, with a more realistic interaction, a computation that is underway and will be reported elsewhere.

As this is numerically more demanding, we resort to the AM, defined in Eq. (24). In Figs. (3 and 4), the numerical results for $G_{\gamma\gamma^*\eta_c}$ and $Q^2G_{\gamma\gamma^*\eta_c}$, respectively, contain the plots obtained through employing the AM, Eq. (24); perturbative QCD calculation [75]; and *BABAR* data. As can be seen from these figures, the AM produces results which agree well with experiment for all the range of Q^2, where results are available. Moreover, it behaves like $1/Q^2$ for large Q^2 and matches the perturbative QCD limit of the TFF.

V. η_c PARTON DISTRIBUTION AMPLITUDE

The perturbative calculation of the $\eta_c \to \gamma\gamma^*$ TFF in Ref. [75] is based upon a factorization of short- and long-distance physics. In other words, it is a convolution of a hard-scattering amplitude computed perturbatively from QCD and a universal hadronic light-cone wave function. This wave function cannot be determined completely accurately, but the η_c decay constant, which probes the wave function at origin, can provide stringent constraints on the latter. On the other hand, the PDA is also connected to the wave function, the former being the integration of the latter over the transverse momentum. This interconnection was exploited in Ref. [75] to propose the parametrization for the η_c PDA for all spacelike values of Q^2,

$$\phi(x) = N_\phi(a)x(1-x)\exp\left[-a^2 m_{\eta_c}^2 (x-x_0)^2\right], \qquad (35)$$

where $N_\phi(a)$ is fixed such that $\int_0^1 dx\phi(x) = 1$ and $x_0 = 1/2$. The conformal limit of this meson parton distribution amplitude $\phi^{asy}(x) = 6x(1-x)$ is obtained formally in the limit $am_{\eta_c} \to 0$).

In Ref. [75], the determination of the η_c decay constant suggests the value $a = 0.97$ GeV^{-1} for the transverse size parameter. This value is also consistent with the estimates for the charge radius squared or the quark velocity in potential models [76]. The behavior of the PDA, Eq. (35), plotted in Fig. 5, resembles the theoretically expected and experimentally confirmed behavior of heavy-hadron fragmentation functions; see Ref. [75] and references therein.

In our current work, we refer to the novel method, developed in Ref. [45], to compute the meson PDA from the projection onto the light front of the meson's Poincaré-covariant Bethe-Salpeter wave function. Carrying out this exercise for the AM, Eq. (24), produces $a \cong 1$ GeV^{-1}. Note that the values of a and $\sigma = m_\pi/m_{\eta_c}$, used in defining the AM, are correlated: a small value of σ gives a closer to 1 while a value ≈ 1 recovers the PDA of the pion obtained with the AM.

This computation produces plots displayed in Fig. 5. In the same figure, we also present the AM result for the PDA, evolved from 4 to 50 GeV^2 through the leading-order QCD Efremov-Radyushkin-Brodsky-Lepage (ERBL) evolution equation [78–81]. Interestingly, the AM result is practically indistinguishable from the result of Ref. [75]. For the sake

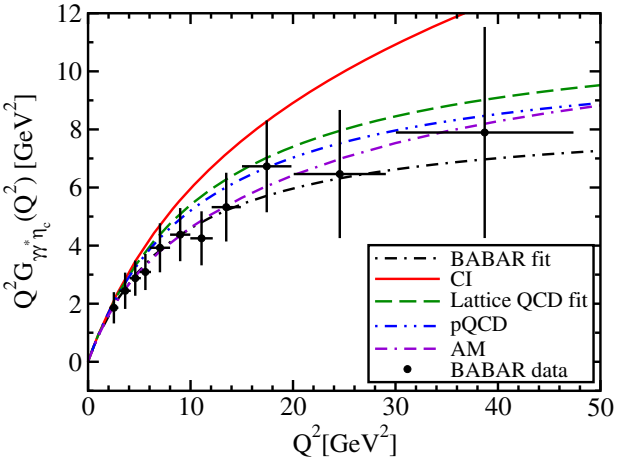

FIG. 4. Numerical results for $Q^2G_{\gamma^*\gamma\eta_c}$. See the caption for Fig. 3.

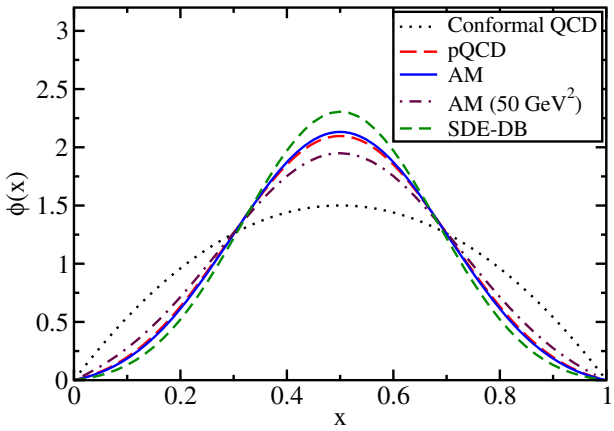

FIG. 5. Numerical results for the η_c PDA, $\phi(x)$, obtained with the AM. We have also plotted the resulting PDA evolved to 50 GeV^2, using the leading-order QCD ERBL evolution equation (see text). For the sake of comparison, we have also included the perturbative QCD (pQCD) results of Ref. [75], the asymptotic QCD expression $6x(1-x)$ (Conformal QCD), and the recent SDE prediction (SDE-DB) of Ref. [77].

of comparison, we also superimpose the result reported in Ref. [77], obtained with a sophisticated DCSB-improved SDE truncation (SDE-DB).

Together with the results for the form factors, this analysis essentially means that the SDE-based AM already encodes a reliable description of the η_c meson and that a full numerical calculation with a realistic interaction should reproduce similar results.

VI. CONCLUSIONS

We have computed the EFF and the TFF $[\eta_c(1S) \to \gamma\gamma^*]$ for the η_c meson, and the corresponding charge radii, in a CI as well as an SDE-BSE formalism inspired AM. Within the CI, we employ the dressing of the quark-photon vertex, consistent with the model truncation and the WTI. It ensures the form factor possesses a vector meson pole at $Q^2 = -m^2_{J/\Psi}$. Since the mass $m_{J/\Psi}$ is large, the effect of the meson vector pole on the charge radii is very small; i.e., the heavier the meson, the closer it is to a point particle. Our CI is based upon a good description of the masses of the ground state in four different channels: pseudoscalar $[\eta_c(1S)]$, vector $[J/\Psi(1S)]$, scalar $[\chi_{c_0}(1P)]$, and axial vector $[\chi_{c_1}(1P)]$, as well as the weak decay constants of the $\eta_c(1S)$ and $J/\Psi(1S)$ and the charge radius of $\eta_c(1S)$.

For the form factors, expectedly, the CI results agree with QCD-based prediction and/or experiments only up to a certain value of the virtual photon momentum transfer Q^2. This observation is in line with earlier similar calculations for the π and the ρ [19–21], where it is argued that the form factors of hadrons in a CI are harder than the real QCD-based results. Therefore, for the CI, both form factors tend to a constant for $Q^2 \to \infty$, which is a consequence of the momentum-independent interaction.

Furthermore, we have also extended an SDE-BSE based AM, proposed for the light-quark sector, to study the η_c. We calculate EFF, TFF $[\eta_c(1S) \to \gamma\gamma^*]$, and also the η_c PDA with this model. For the EFF, the results are in excellent agreement with the lattice findings for all Q^2 available. An extra advantage of the AM is that its simplicity allows us to extend the computation to any desired values of spacelike Q^2. We show the results till $Q^2 = 15$ GeV^2 for the EFF. For the TFF $[\eta_c(1S) \to \gamma\gamma^*]$, we calculate the results till $Q^2 = 50$ GeV^2. For all the regime of momentum transfer squared Q^2, the results match perfectly with the experiment. Moreover, for large Q^2, the perturbative QCD limit of Ref. [75] is faithfully reproduced.

This essentially means that the AM already gives a good description of the η_c meson and that a full numerical calculation with a realistic interaction should be able to produce similar results. We are currently in the process of extending our work to the sector of bottomonia.

ACKNOWLEDGMENTS

The authors acknowledge financial support from CONACyT, México (doctoral scholarship for M. A. Bedolla and K. Raya; postdoctoral Contract No. 290917-UMSNH for J. J. Cobos-Martínez, and research Grant No. CB-2014-242117 for A. Bashir). This work has also partly been financed by the CIC-UMSNH Grant No. 4.10.

[1] P. Jain and H. J. Munczek, Phys. Rev. D **48**, 5403 (1993).
[2] P. Maris, C. D. Roberts, and P. C. Tandy, Phys. Lett. B **420**, 267 (1998).
[3] P. Maris and P. C. Tandy, Phys. Rev. C **60**, 055214 (1999).
[4] P. Boucaud, J. P. Leroy, A. L. Yaouanc, J. Micheli, O. Pène, and J. Rodríguez-Quintero, J. High Energy Phys. 06 (2008) 099.
[5] A. Aguilar, D. Binosi, and J. Papavassiliou, Phys. Rev. D **78**, 025010 (2008).
[6] M. Pennington and D. Wilson, Phys. Rev. D **84**, 119901 (2011).
[7] L. Chang and C. D. Roberts, Phys. Rev. Lett. **103**, 081601 (2009).
[8] A. Kizilersu and M. Pennington, Phys. Rev. D **79**, 125020 (2009).
[9] A. Bashir, R. Bermudez, L. Chang, and C. Roberts, Phys. Rev. C **85**, 045205 (2012).
[10] M. Gomez-Rocha, T. Hilger, and A. Krassnigg, Phys. Rev. D **93**, 074010 (2016).
[11] M. J. Aslam, A. Bashir, and L. X. Gutierrez-Guerrero, Phys. Rev. D **93**, 076001 (2016).
[12] A. Bashir, C. Calcaneo-Roldan, L. X. Gutierrez-Guerrero, and M. E. Tejeda-Yeomans, Phys. Rev. D **83**, 033003 (2011).
[13] A. Bashir, A. Raya, and S. Sanchez-Madrigal, Phys. Rev. D **84**, 036013 (2011).
[14] A. Bashir and R. Delbourgo, J. Phys. A **37**, 6587 (2004).
[15] P. Maris and P. C. Tandy, Phys. Rev. C **62**, 055204 (2000).
[16] P. Maris and P. C. Tandy, Phys. Rev. C **65**, 045211 (2002).
[17] M. S. Bhagwat and P. Maris, Phys. Rev. C **77**, 025203 (2008).
[18] G. M. Huber *et al.* (Jefferson Lab Collaboration), Phys. Rev. C **78**, 045203 (2008).
[19] L. Gutierrez-Guerrero, A. Bashir, I. Cloet, and C. Roberts, Phys. Rev. C **81**, 065202 (2010).
[20] H. Roberts, C. Roberts, A. Bashir, L. Gutierrez-Guerrero, and P. Tandy, Phys. Rev. C **82**, 065202 (2010).
[21] H. Roberts, A. Bashir, L. Gutierrez-Guerrero, C. Roberts, and D. Wilson, Phys. Rev. C **83**, 065206 (2011).

[22] K. Raya, L. Chang, A. Bashir, J. J. Cobos-Martinez, L. X. Gutiérrez-Guerrero, C. D. Roberts, and P. C. Tandy, Phys. Rev. D **93**, 074017 (2016).
[23] A. Krassnigg and P. Maris, J. Phys. Conf. Ser. **9**, 153 (2005).
[24] M. Bhagwat, A. Krassnigg, P. Maris, and C. Roberts, Eur. Phys. J. A **31**, 630 (2007).
[25] P. Maris and P. Tandy, Nucl. Phys. B, Proc. Suppl. **161**, 136 (2006).
[26] M. Blank and A. Krassnigg, Phys. Rev. D **84**, 096014 (2011).
[27] P. Maris, AIP Conf. Proc. **892**, 65 (2007).
[28] A. Krassnigg, Phys. Rev. D **80**, 114010 (2009).
[29] M. Bhagwat, A. Holl, A. Krassnigg, C. Roberts, and P. Tandy, Phys. Rev. C **70**, 035205 (2004).
[30] N. Souchlas, Phys. Rev. D **81**, 114019 (2010).
[31] E. Rojas, B. El-Bennich, and J. de Melo, Phys. Rev. D **90**, 074025 (2014).
[32] M. A. Bedolla, J. Cobos-Martinez, and A. Bashir, Phys. Rev. D **92**, 054031 (2015).
[33] C. S. Fischer, S. Kubrak, and R. Williams, Eur. Phys. J. A **51**, 10 (2015).
[34] S. Kubrak, C. S. Fischer, and R. Williams, J. Phys. Conf. Ser. **599**, 012013 (2015).
[35] T. Hilger, C. Popovici, M. Gómez-Rocha, and A. Krassnigg, Phys. Rev. D **91**, 034013 (2015).
[36] J. J. Dudek, R. G. Edwards, and D. G. Richards, Phys. Rev. D **73**, 074507 (2006).
[37] J. J. Dudek, R. G. Edwards, N. Mathur, and D. G. Richards, J. Phys. Conf. Ser. **69**, 012006 (2007).
[38] J. Dudek and A. Szczepaniak, AIP Conf. Proc. **814**, 587 (2006).
[39] V. P. Druzhinin (*BABAR* Collaboration), Proc. Sci., **ICHEP2010**, 144 (2010).
[40] C. Chen, L. Chang, C. D. Roberts, S. Wan, and D. J. Wilson, Few Body Syst. **53**, 293 (2012).
[41] H. L. Roberts, L. Chang, I. C. Cloet, and C. D. Roberts, Few Body Syst. **51**, 1 (2011).
[42] A. Bashir, L. Chang, I. C. Cloët, B. El-Bennich, Y.-X. Liu, C. D. Roberts, and P. C. Tandy, Commun. Theor. Phys. **58**, 79 (2012).
[43] G. Eichmann, R. Alkofer, I. Cloet, A. Krassnigg, and C. Roberts, Phys. Rev. C **77**, 042202 (2008).
[44] I. Cloet, A. Krassnigg, and C. Roberts, in *11th International Conference on Meson-Nucleon Physics and the Structure of the Nucleon (MENU2007)*, eConf C070910, 125 (2007).
[45] L. Chang, I. C. Cloet, J. J. Cobos-Martinez, C. D. Roberts, S. M. Schmidt, and P. C. Tandy, Phys. Rev. Lett. **110**, 132001 (2013).
[46] L. Chang, C. Mezrag, H. Moutarde, C. D. Roberts, J. Rodríguez-Quintero, and P. C. Tandy, Phys. Lett. B **737**, 23 (2014).
[47] C. Mezrag, L. Chang, H. Moutarde, C. D. Roberts, J. Rodríguez-Quintero, F. Sabatié, and S. M. Schmidt, Phys. Lett. B **741**, 190 (2015).
[48] F. Gross, *Relativistic Quantum Mechanics and Field Theory*, 1st ed. (Wiley, New York, 1993).
[49] E. E. Salpeter and H. A. Bethe, Phys. Rev. **84**, 1232 (1951).
[50] M. Gell-Mann and F. Low, Phys. Rev. **84**, 350 (1951).
[51] I. G. Aznauryan *et al.*, Int. J. Mod. Phys. E **22**, 1330015 (2013).
[52] C. D. Roberts, M. S. Bhagwat, A. Holl, and S. V. Wright, Eur. Phys. J. Spec. Top. **140**, 53 (2007).
[53] A. Holl, C. D. Roberts, and S. V. Wright, arXiv:nucl-th/0601071.
[54] P. Maris and C. D. Roberts, Int. J. Mod. Phys. E **12**, 297 (2003).
[55] R. Alkofer and L. von Smekal, Phys. Rep. **353**, 281 (2001).
[56] Ph. Boucaud, J. P. Leroy, A. Le Yaouanc, J. Micheli, O. Pène, and J. Rodríguez-Quintero, Few Body Syst. **53**, 387 (2012).
[57] D. Ebert, T. Feldmann, and H. Reinhardt, Phys. Lett. B **388**, 154 (1996).
[58] C. Roberts, Prog. Part. Nucl. Phys. **61**, 50 (2008).
[59] R. Farias, G. Dallabona, G. Krein, and O. Battistel, Phys. Rev. C **73**, 018201 (2006).
[60] R. Farias, G. Dallabona, G. Krein, and O. Battistel, Phys. Rev. C **77**, 065201 (2008).
[61] C. H. Llewellyn-Smith, Ann. Phys. (N.Y.) **53**, 521 (1969).
[62] E. Follana, Q. Mason, C. Davies, K. Hornbostel, G. P. Lepage, J. Shigemitsu, H. Trottier, and K. Wong (HPQCD and UKQCD Collaborations), Phys. Rev. D **75**, 054502 (2007).
[63] M. Kalinowski and M. Wagner, *Proc. Sci.*, LATTICE2013, 241 (2014).
[64] P. Maris and C. D. Roberts, Phys. Rev. C **56**, 3369 (1997).
[65] A. Ayala, A. Bashir, D. Binosi, M. Cristoforetti, and J. Rodriguez-Quintero, Phys. Rev. D **86**, 074512 (2012).
[66] A. Bashir, A. Raya, and J. Rodriguez-Quintero, Phys. Rev. D **88**, 054003 (2013).
[67] K. Nakamura and P. D. Group, J. Phys. G **37**, 075021 (2010).
[68] C. T. H. Davies, C. McNeile, E. Follana, G. P. Lepage, H. Na, and J. Shigemitsu, Phys. Rev. D **82**, 114504 (2010).
[69] G. C. Donald, C. T. H. Davies, R. J. Dowdall, E. Follana, K. Hornbostel, J. Koponen, G. P. Lepage, and C. McNeile, Phys. Rev. D **86**, 094501 (2012).
[70] I. C. Cloët, L. Chang, C. D. Roberts, S. M. Schmidt, and P. C. Tandy, Phys. Rev. Lett. **111**, 092001 (2013).
[71] V. M. Braun *et al.*, Phys. Rev. D **74**, 074501 (2006).
[72] F. T. Hawes and M. A. Pichowsky, Phys. Rev. C **59**, 1743 (1999).
[73] P. Maris and P. C. Tandy, Phys. Rev. C **61**, 045202 (2000).
[74] P. Maris, arXiv:nucl-th/0209048.
[75] T. Feldmann and P. Kroll, Phys. Lett. B **413**, 410 (1997).
[76] W. Buchmuller and S. H. H. Tye, Phys. Rev. D **24**, 132 (1981).
[77] M. Ding, F. Gao, L. Chang, Y.-X. Liu, and C. D. Roberts, Phys. Lett. B **753**, 330 (2016).
[78] A. Efremov and A. Radyushkin, Mod. Phys. Lett. A **24**, 2803 (2009).
[79] A. V. Efremov and A. V. Radyushkin, Phys. Lett. **94B**, 245 (1980).
[80] G. P. Lepage and S. J. Brodsky, Phys. Lett. **87B**, 359 (1979).
[81] G. P. Lepage and S. J. Brodsky, Phys. Rev. D **22**, 2157 (1980).